REPRODUCTION
RESEARCH

Protein profile screening: reduced expression of *Sord* in the mouse epididymis induced by nicotine inhibits tyrosine phosphorylation level in capacitated spermatozoa

Jingbo Dai*, Wangjie Xu*, Xianglong Zhao, Meixing Zhang, Dong Zhang, Dongsheng Nie, Min Bao, Zhaoxia Wang, Lianyun Wang and Zhongdong Qiao

School of Life Sciences and Biotechnology, Shanghai Jiao Tong University, Shanghai 200240, People's Republic of China

Correspondence should be addressed to Z Qiao; Email: zdqiao@sjtu.edu.cn

*(J Dai and W Xu contributed equally to this work)

Abstract

Many studies have revealed the hazardous effects of cigarette smoking and nicotine exposure on male fertility, but the actual, underlying molecular mechanism remains relatively unclear. To evaluate the detrimental effects of nicotine exposure on the sperm maturation process, two-dimensional gel electrophoresis and mass spectrometry analyses were performed to screen and identify differentially expressed proteins from the epididymal tissue of mice exposed to nicotine. Data mining analysis indicated that 15 identified proteins were mainly involved in the molecular transportation process and the polyol pathway, indicating impaired epididymal secretory functions. Experiments *in vitro* confirmed that nicotine inhibited tyrosine phosphorylation levels in capacitated spermatozoa via the downregulated seminal fructose concentration. *Sord*, a key gene encoding sorbitol dehydrogenase, was further investigated to reveal that nicotine induced hyper-methylation of the promoter region of this gene. Nicotine-induced reduced expression of *Sord* could be involved in impaired secretory functions of the epididymis and thus prevent the sperm from undergoing proper maturation and capacitation, although further experiments are needed to confirm this hypothesis.

Reproduction (2016) **151** 227–237

Introduction

As one of the most common public health issues in the world, tobacco consumption is directly responsible for nearly 6 million deaths annually, and another 600 000 people die each year due to second-hand smoke (Yach 2014). Many lifestyle choices, such as tobacco smoking, have long been considered as impairments of male fertility (Girela *et al.* 2013). Epidemiological and clinical studies have discovered significant declines in sperm density, sperm mobility, semen volume (Künzle *et al.* 2003, Ramlau-Hansen *et al.* 2007) and the percentage of normal sperm morphology in smoking populations (Trummer *et al.* 2002, Gaur *et al.* 2007). These studies provided a direct understanding of the hazardous effects of smoking on male fertility, but the detailed molecular mechanism underlying remains relatively unclear, partly due to the complexity of chemical components in tobacco smoke (Dai *et al.* 2015*a*).

Nicotine is one of the most significant hazardous substances in tobacco smoke (Editorial 2014) and it can be detected in smokers' serum and semen (Pacifici *et al.* 1995). The *in vivo* toxicological effects of nicotine have been assessed in many animal studies. In the male reproductive system, nicotine (0.5 mg/kg) can decrease sperm motility and count as well as increase the percentage of sperm abnormalities in rats (Oyeyipo *et al.* 2011, Ezzatabadipour *et al.* 2012). A more comprehensive study assessed testicular gametogenesis, steroidogenesis and the expression of steroidogenic acute regulatory proteins in nicotine-treated rats. Activity of testicular androgenic enzymes, intratesticular and plasma testosterone concentrations, and plasma gonadotropin concentrations were significantly reduced, along with an alteration in the testicular antioxidant status and spermatogenesis dysfunction, which were indicated by a significant reduction in the number of different generations of germ cells at specific stages in the spermatogenesis cycle (Jana *et al.* 2010). These results indicate the comprehensive effects of nicotine on male reproduction, which involves oxidative stress

ISSN 1470–1626 (paper) 1741–7899 (online)
DOI: 10.1530/REP-15-0370
Online version via www.reproduction-online.org

in the gonads and dysfunction of the reproductive hormone system.

The major functions of the epididymis are sperm transport, storage, concentration and maturation (Cooper & Yeung 2006). During transit in the epididymal duct, sperm maturation involves the acquisition of forward motility and the fertilizing ability (Jones 1999). The major modifications of spermatozoa in the epididymal lumen include: increases in disulfide bonds and net surface negative charge; changes in membrane phospholipid composition and the cholesterol/phospholipid ratio; relocation of surface antigens; and modifications of sperm surface proteins (Rodriguez *et al*. 2002, Dacheux & Dacheux 2014). Detached ciliary tufts (DCTs) in semen originate from the epididymal epithelium and are closely associated with biochemical evidence of epididymal dysfunction (González-Jiménez & Villanueva-Díaz 2006). DCTs in semen are also associated with a high incidence of tobacco consumption (Bornman *et al*. 1989), and this finding may shed light on the role of epididymal involvement as a result of reproductive pathology caused by tobacco smoking. Zhu *et al*. (2013) utilized proteomic analysis to screen differentially expressed proteins (DEPs) in the mouse epididymis treated with tobacco smoke, and identified 27 proteins that showed significant alterations in their expressive levels. Most of these DEPs participate in energy metabolism, protein processing and oxidative stress process. This result suggests a presumable mechanism of epididymal impairment due to tobacco smoking.

To further investigate the exact molecular mechanisms of nicotine-induced impairment of male fertility and the effects of nicotine on epididymal functions, a nicotine exposure animal model was created by injecting sexually mature male mice with nicotine throughout a spermatogenesis cycle. Proteomic methods were used to illustrate the impact of nicotine on the protein expression profile of the mouse epididymis. To identify the molecular mechanism by which such changes occur, promoter DNA methylation levels of some key genes were also examined in our study.

Materials and methods

Animal treatments and sample collection

The animal experiments in this study were approved by the Bioethics Committee of Shanghai Jiao Tong University. Sixty 6-week-old male C57BL/6J mice (acquired from Shanghai SLAC Laboratory Animal Co. Ltd, Shanghai, China) were randomly divided into a control group and a nicotine-treated group of 30 mice each. The nicotine-treated group received a dose of 0.2 mg free-base nicotine/100 g daily via i.p. injection to mimic the blood plasma levels of nicotine in heavy smokers ($\geq$20 cigarettes/day) (Matta *et al*. 2007). The control group received a daily equivalent of saline. All animals were housed at room temperature with a ratio of 12 h light:12 h darkness in an air-conditioned environment. After 5 weeks of treatment, the two groups of mice were euthanized using cervical dislocation, and the epididymal and spermatozoal samples were collected. The whole epididymides of 20 mice from each group were collected for DNA/RNA/protein extraction and further experiments were performed. For the remaining ten mice in each group, the caput, corpus and cauda epididymides were collected separately. The epididymal segments were fixed in 4% polyformaldehyde and immersed sequentially in gradient ethanol for 24 h and then embedded in paraffin. The paraffin-embedded tissue samples were sectioned at 4 μm for immunofluorescence (IF).

Cell lines, chemicals and antibodies

Crl-2053 cell line derived from the mouse testis were cultured in DMEM supplemented with 50 IU/ml penicillin, 50 μg/ml streptomycin and 10% fetal bovine serum (FBS) at 37 °C, 5% CO_2. After Crl-2053 cells were cultured to 90–95% confluency, 5-aza-2′-deoxycytidine (5′-aza-dC) (Sigma) was added to the culture medium to reach final concentrations of 0, 0.5, 1 and 2 μM. The cells were harvested with TRIzol (Life Technologies) following 48 h of treatment, and the total mRNA, total protein and genomic DNA were obtained according to standard protocols.

Two-dimensional gel electrophoresis

Cell lysis buffer (9.5 M urea, 4% CHAPS, 2% DTT, 0.5%, immobilized pH gradient (IPG) buffer and protease inhibitor mix) was added to the epididymal samples, and tissue homogenates were then generated. The homogenates were sonicated for 15 min to break up the cells completely. The insoluble material was then removed after the mixture was centrifuged at 20 000 ***g*** at 4 °C for 45 min. For two-dimensional gel electrophoresis (2-DE), five samples were pooled in each gel and each group contained three biological replicates. Protein samples (100 and 400 μg) were loaded on each analytical and preparative gel. Isoelectric focusing was performed using a four-step program consisting of 12 h at 30 V, 1 h at 500 V, 1 h at 1000 V, and 8 h at 8000 V with pH 3–10 IPG strips (13 cm, nonlinear; Amersham) and an Ettan IPGphor Isoelectric Focusing System (GE Amersham Biosciences). The IPG strips were equilibrated for 10 min in 50 mM Tris–HCl (pH 8.8), 6 M urea, 2% SDS, 30% glycerol, 1% DTT and trace bromophenol blue, followed by 10 min of equilibration in the same buffer, but with 2.5% iodoacetamide in place of 1% DTT. The strips were then transferred to the top of pre-cast 12.5% SDS–polyacrylamide gels. A Hofer SE 600 system (GE Amersham Biosciences) was used to perform gel electrophoresis for 30 min at 15 mA/gel, followed by 65 min at 30 mA/gel.

A modified silver staining method, which was compatible with subsequent mass spectrometric analysis, was used to visualize the separated protein spots in the analytical gels. The silver-stained gels were digitized by scanning with a UMax Powerlook 2110XL system (UMax, Dallas, TX, USA), and image analysis was performed using ImageMaster 2D Platinum (GE Amersham Biosciences). Spot detection and matching were performed automatically with subsequent manual editing

and review to ensure a higher level of reproducibility between the normalized spot volumes of gels from the three replicates. Student's t test ($P<0.05$) was used to identify significantly differentially expressed protein spots that demonstrated at least a 1.5-fold change in expression level.

Matrix-assisted laser desorption/ionization time-of-flight mass spectrometry

Differentially expressed protein spots were manually excised from the SDS–polyacrylamide gels, and tryptic digestion of proteins was performed to release the peptides. Dehydrated peptide samples were reconstituted in 2 μl of 20% ACN and spotted on a 384-well Opti-TOF stainless steel plate. Before drying, the plate was covered with matrix solution containing 5 mg/ml cyano-4-hydroxycinnamic acid (Sigma) in 50% ACN with 0.1% trifluoroacetic acid. Positive ion mass spectra for protein identification were obtained using a 4800 Proteomics Analyzer (Applied Biosystems). MS spectra were recorded in reflector mode over a mass range of 800–4000 m/z and calibrated using an adjacent spot containing six known peptides. Up to ten of the most intense ion signals were selected as precursors for MS/MS acquisition, excluding the trypsin autolysis peaks and the matrix ion signals. In MS/MS positive ion mode, 50 subspectra with 50 shots per subspectrum were accumulated for one main MS spectrum using a random search pattern. The collision gas used was air, the collision energy was 2 kV, and the default calibration was set using the Glu1-Fibrinopeptide B spotted onto Cal 7 positions of the MALDI target. Combined peptide mass fingerprinting and MS/MS queries were performed using the MASCOT search engine 2.2 (Matrix Science, Ltd, Boston, MA, USA) embedded into GPS-Explorer Software 3.6 (Applied Biosystems) for database searching (IPI Mouse, Cambridgeshire, UK) with the following parameter settings: 100 ppm mass accuracy was used; one missed trypsin cleavage was allowed; carbamidomethylation was set as a fixed modification; and the oxidation of methionine was allowed as a variable modification. A MS/MS fragment tolerance of 0.8 Da and a peptide tolerance of 250 ppm were used, and the significance threshold was set at $P<0.05$.

Comparative proteomic analysis

We identified and categorized the molecular functions, biological processes and cellular components represented in the DEPs in our datasets according to their functions and locations. The mRNA sequences of the identified proteins in FASTA format were obtained from the National Center for Biotechnology Information (NCBI) (http://www.ncbi.nlm.nih.gov/). Gene ontology annotations for the identified proteins based on BLAST results were performed using Blast2GO (www.blast2go.de). After uploading the differentially expressed protein list onto the WEB-based GEne SeT AnaLysis Toolkit (WebGestalt) server (http://bioinfo.vanderbilt.edu/webgestalt/analysis.php), the involved pathway networks were determined. Gene identifiers corresponding to the DEPs were identified, and the dataset was analyzed using Ingenuity Pathway Analysis (IPA; Ingenuity Systems, www.ingenuity.com).

Western blot analysis

Purified protein samples were isolated from the epididymal tissues using TRIzol reagent (Invitrogen) and subjected to SDS–PAGE. The resolved polypeptides were electrophoretically transferred onto the PVDF membranes at 15 V for 1 h in 25 mM Tris–HCl, 192 mM glycine and 20% (v/v) methanol. The PVDF membranes were blocked with 5% skimmed milk in TBST (100 mM Tris-buffered saline, pH 7.4, 0.1% Tween-20) for 1 h at room temperature, followed by incubation with primary antibodies in TBST for 1 h at 4 °C overnight. After rinsing three times with TBST, the membranes were incubated with secondary antibody (goat anti-rabbit IgG-HRP, Maibio, Cat No. HSA0004, 1:20 000 in TBST) at room temperature for 1 h. Finally, the PVDF membranes were rinsed three times with TBST. HRP was detected using the Millipore Immobilon Western Chemiluminescent HRP substrate, and the final blots were exposed to X-ray film. The expression levels of the target genes were normalized against the internal reference protein GAPDH. Western blot analyses in this study were conducted at least with three biological replicates. The primary antibodies used in western blot analysis were as follows: ODF2 rabbit polyAb (Proteintech Group, Cat No. 12058-1-AP); TAGLN rabbit polyAb (Proteintech Group, Cat No. 10493-1-AP); MDH1 rabbit polyAb (Proteintech Group, Cat No. 15904-1-AP); SORD rabbit polyAb (Proteintech Group, Cat No. 15881-1-AP); Vim rabbit polyAb (Proteintech Group, Cat No. 10366-1-AP); and GAPDH Rabbit mAb (Cell Signal Technology, Cat No. 2118S).

Real-time PCR

RNA samples were isolated from the epididymis of the nicotine-treated and control groups using TRIzol reagent and reverse-transcribed into cDNA with Fermentas RevertAid reverse transcriptase (Fermentas EP0441). Quantitative real-time PCR was performed using the Bestar real-time PCR mastermix (SybrGreen; DBI Bioscience, Ludwigshafen, Germany) and the ABI PRISM 7500 system (Applied Biosystems), following the manufacturers' protocols. The primers for real-time PCR were designed via Primer-blast (http://www.ncbi.nlm.nih.gov/tools/primer-blast/) and synthesized by Invitrogen. The transcript levels of the target genes were normalized against the internal reference gene *Gapdh*. Relative quantification (RQ) was performed using the $2^{-\Delta(\Delta Ct)}$ method (Pfaffl *et al.* 2004), where RQ or the fold change is equal to $2^{-((\text{Mean } \Delta Ct \text{ target})-(\text{Mean } \Delta Ct \text{ calibrator}))}$.

Immunofluorescence

The tissue sections of the caput, corpus and cauda epididymides were baked at 85 °C for 15 min and then deparaffinized in xylene, followed by rehydration in a series of decreasing ethanol concentrations. The rehydrated sections were washed with flowing water, and 0.01 M citrate buffer (pH 6.0) was used for antigen retrieval in a pressure cooker. The sections were then treated with 1% Triton X-100 for 15 min and incubated with 5% BSA (in TBS, pH 7.4) for 30 min. This procedure was followed by rinsing with TBS and an overnight incubation with

the rabbit anti-SORD antibody (Proteintech Group, Cat No. 11980-1-AP, 1:50 in TBS) and mouse anti-CD52 antibody (Abcam, Cat No. ab2576, 1:20 in TBS) at 4 °C. After washing with TBS, the sections were incubated with FITC-conjugated anti-rabbit IgG (Proteintech Group, Cat No. SA00003-2, 1:200 in TBS) and TRITC-conjugated anti-mouse IgG (Proteintech Group, Cat No. SA00007-1, 1:100 in TBS) at 37 °C for 1 h. Lastly, the sections were mounted with DAPI mounting medium after washing with TBS three times for 5 min each. Fluorescence images were recorded with a Leica DM3500 fluorescence microscope.

Spermatozoal purification and in vitro *capacitation*

After the mice were euthanized using cervical dislocation, the cauda epididymis was carefully isolated and the spermatozoa were forced out. The isolated spermatozoa were suspended in human tubal fluid (HTF) medium for subsequent treatments. The spermatozoa suspended in HTF medium were then purified through the swim-up method in Earle's balanced salt solution (EBSS) containing 10% (v/v) FBS. The selected spermatozoa were pelleted through centrifugation at 1000 ***g*** and 4 °C for 15 min, followed by washing three times with PBS. Purified spermatozoa were then suspended at a concentration of 10^6/ml in enriched Krebs–Ringer bicarbonate (EKRB) solution containing 3 mg/ml BSA and then incubated at 37 °C, 5% CO_2 and 95% air for 2 h to complete *in vitro* capacitation. EKRB without BSA was used to suspend spermatozoa, which were considered as negative controls. The capacitated spermatozoa were used for cell lysis and total protein was consequently extracted. Tyrosine phosphorylation was measured by western blotting (phosphotyrosine rabbit polyAb, Gene Tex, Irvine, CA, USA, Cat No. 821200775) to detect the efficiency of sperm capacitation.

Bisulfite sequencing PCR and methylation-specific PCR

Genomic DNA samples (1 μg) isolated from the epididymis were treated with the Methylamp DNA Modification Kit (Epigentek, New York, NY, USA), as described in the manufacturer's instructions. After modification, the eluted DNA (5 μl) was PCR amplified with *Sord*-specific bisulfate sequencing primers (Sord-BSP-S 5′-TTTTGGTTTGTTAAGTTT-GAGTGAA-3′ and Sord-BSP-A 5′-TACACCACCAAAAA-CAAATTCTC-3′). The PCR product (268 bp) was purified and then cloned into the pMD19-T vector (TaKaRa, Kyoto, Japan). After being transformed into competent bacteria, ten clones from each group were sequenced. For methylation-specific PCR (MSP), genomic DNA samples were isolated from 5′-aza-dC-treated Crl-2053 cells using the phenol–chloroform method and then treated with sodium bisulfate. The treated DNA (2.5 μl) was amplified with two sets of MSP primers (Sord-M-S 5′-AAGTTTGAGTGAAGTTTCGTTTTTC-3′ and Sord-M-A 5′-TACTCTCTTACTTCGAAATATCCGC-3′; Sord-U-S 5′-GTTT-GAGTGAAGTTTT-GTTTTTTGT-3′ and Sord-U-A 5′-ACTCTCT-TACTTCAAAATATCCACT-3′). For bisulfite sequencing PCR (BSP) and MSP, touchdown PCR was performed with EX-Taq HS (TaKaRa) at an annealing temperature from 60 to 55 °C to ensure specific PCR amplification. PCR products with 263 bp were resolved using 2% agarose gel electrophoresis. BSP analyses were conducted in three biological replicates to acquire convincing results.

Statistical analyses

All statistical analyses were performed using SPSS version 19.0. The data in this study are presented as mean value ± S.D. Student's *t* test (two-tailed distribution with a two-sample equal variance) was used to compare the results between the two groups. Differences were considered significant at $P<0.05$ and $P<0.01$ (indicated by * and ** respectively).

Results

Nicotine exposure altered protein profile in the mouse epididymal tissue

To investigate alterations of the protein profile in the mouse epididymis induced by nicotine exposure, soluble protein samples from the control and nicotine-treated groups were compared using the 2-DE technique. Three replicates (six gels) were performed for each sample. From the over 1000 spots detected in the 2-DE analysis (Fig. 1), 15 spots (≥1.5-fold, $P<0.05$) that showed significant differences in expressive levels between the two groups were chosen for further analysis. Basic information of the proteins successfully identified by matrix-assisted laser desorption/ionization time-of-flight mass spectrometry (MALDI-TOF-MS) is given in Table 1. Among these DEPs, seven were upregulated and eight were downregulated in the nicotine-treated group compared with the control. The upregulated proteins include Na^+/H^+ exchange regulatory cofactor (NHE-RF3), cysteine-rich secretory protein 1 precursor (CRISP1), keratin 8 or EndoA cytokeratin (KRT8), transgelin (TAGLN), vimentin (VIM), lectin, galactose binding, soluble 3 (LGALS3) and aconitate hydratase, mitochondrial precursor (ACO2). The downregulated proteins include heat shock protein 5 (HSPA5),ATP synthase subunit beta mitochondrial precursor (ATP5B), sorbitol dehydrogenase (SORD), malate dehydrogenase 1 (MDH1), carboxypeptidase Q (CPQ) (plasma glutamate carboxypeptidase (PGCP)), heat shock 60 kDa protein 1 (HSPD1), outer dense fiber protein 2 isoform c (ODF2) and heat shock protein 5 isoform CRE_b (HSPA5).

Verification of the MS results

Western blot and real-time PCR analyses of five candidate proteins (ODF2, TAGLN, MDH1, SORD and VIM) were performed to validate the protein screening results (Fig. 1C). These proteins were chosen for validation on account of their representative fold-change span and the availability of antibodies. Besides, the five proteins have been proven to play important roles in the murine reproductive system, which can be considered as

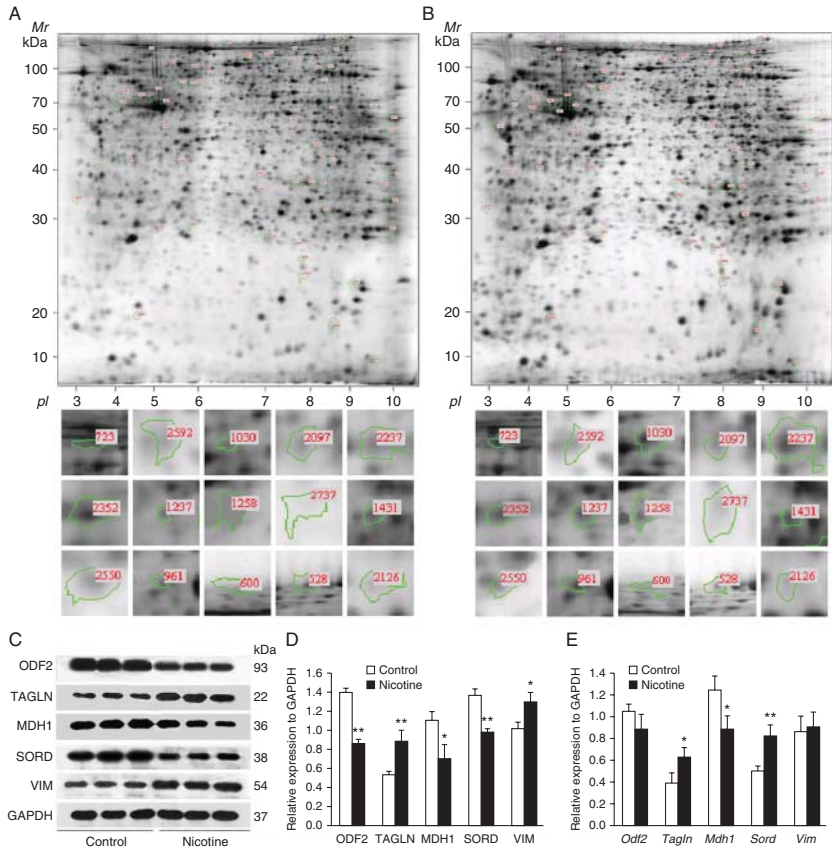

Figure 1 Typical 2-DE maps of the total protein extracted from the mouse epididymis of two groups and the verification analysis of target proteins. (A) Protein extracted from the epididymal samples of the control group. Larger images of the DEP spots are listed below according to the order in Table 1. (B) Protein extracted from the epididymal samples of the nicotine-treated group. (C) Western blot films of the control and nicotine-treated groups. Each group contains three individual biological replicates. (D) Histogram of the western blot results of the control and nicotine-treated groups. The bars represent the mean ± S.D. from three individual experiments. (E) Real-time PCR analysis of the transcripts of DEPs ($n=3$). Relative expression represents a ratio of a specific transcript to that of the internal reference gene *Gapdh*. * indicates significant differences at $P<0.05$ and ** indicates significant differences at $P<0.01$.

promising research targets. Each band of protein from the two groups, which were equilibrated to the expression levels of GAPDH, was measured using densitometric analysis (Fig. 1D). Western blot analysis showed changes in protein expression abundance that closely matched the results from the 2-DE experiment. The expression levels of all of the tested proteins showed a statistically significant difference between the nicotine-treated and control groups (ODF2, $P=0.001$; TAGLN, $P=0.002$; MDH1, $P=0.021$; SORD $P=0.008$; VIM, $P=0.019$). Real-time PCR analysis was also performed to determine whether the transcript levels of the selected genes for each identified protein were altered within the nicotine-treated and control groups (Fig. 1E). The trend for three transcripts was consistent with the results of the 2-DE and MS analysis (*Tagln*, $P=0.036$; *Mdh1*, $P=0.023$; *Sord*, $P=0.002$). The expression levels of the *Odf2* and *Vim* transcripts showed no significant differences between the two groups, which prompted the possibility of post-transcriptional modification of specific genes. These results indicated the reliability of the proteomic results.

Gene ontology and network analysis of identified proteins

For further study, gene ontology annotation was performed. Each identified protein was classified according to GO BLAST and functional annotations. The ontology analysis was conducted by Blast2Go V. 2.6.0 and the results are shown in combined graphics. For the 'biological process' aspect, the identified DEPs were mainly involved in cellular processes, single-organism processes, multicellular organismal processes, response to stimulus, metabolic processes and developmental processes (Fig. 2A). For the 'molecular function' aspect, the DEPs were enriched in the functions of binding and catalytic activity (Fig. 2B). For the 'cellular component' aspect, these DEPs were mainly located in cell, organelle, membrane and macromolecular complexes (Fig. 2C). The sum of the count might exceed 15 because some proteins could be classified into multiple terms.

To gain further insight into the global network functions that differ between the control and nicotine-treated groups, the basic information of the DEPs was uploaded to the IPA server (http://www.ingenuity.com/) and subjected to network analysis. IPA integrates the basic knowledge of genes, chemicals, protein families, processes and pathways based on the interactions and functions derived from the Ingenuity Pathway Knowledge Database. The IPA sever determined a main pathway network (Fig. 2D) that included ten proteins from the 15 DEPs. IPA indicated that the network involves molecular transportation and small molecular biochemistry.

Table 1 Proteins with a significantly higher or lower expression level in the nicotine-treated mouse epididymis compared with the control.

No.	Spot name	Accession number	Identified protein name	Unique peptides	Mascot score	Protein score CI%	Protein MW (Da)	Protein PI	Log2 fold change (N/C)	Fold change	*P*	Major functions
1	723	gi|74220199	Heat shock protein 5 (HSPA5)	31	401	100	72 422	5.07	−1.82	3.53	0.001	Facilitates the assembly of multimeric protein complexes inside the endoplasmic reticulum (ER)
2	2592	gi|22128627	Sorbitol dehydrogenase (SORD)	12	180	100	38 249	6.56	−1.76	3.39	0.001	Converts sorbitol to fructose. Part of the polyol pathway that plays an important role in sperm physiology
3	1030	gi|73621373	Na^+/H^+ exchange regulatory cofactor (NHE-RF3)	13	129	100	56 498	5.29	1.74	3.34	0.001	A scaffold protein that connects plasma membrane proteins and regulatory components
4	2097	gi|31980648	ATP synthase subunit beta (ATP5B)	20	349	100	56 300	5.19	−1.69	3.23	0.003	Mitochondrial membrane ATP synthase produces ATP from ADP in the presence of a proton gradient across the membrane
5	2237	gi|157951659	Cysteine-rich secretory protein 1 precursor (CRISP1)	15	256	100	27 680	6.44	1.45	2.73	0.001	Helps spermatozoa undergo functional maturation while they move from the testis to the ductus deferens
6	2352	gi|387129	Malate dehydrogenase 1 (MDH1)	14	224	100	35 732	5.06	−1.21	2.31	0.012	L-malate dehydrogenase activity
7	1237	gi|309215	Keratin 8 (KRT8)	18	574	100	54 565	5.70	1.14	2.20	0.008	Helps to link the contractile apparatus to dystrophin at the costameres of striated muscle
8	1258	gi|148676915	Carboxypeptidase Q (CPQ)	14	133	100	84 574	8.05	−1.09	2.13	0.025	May play an important role in the hydrolysis of circulating peptides
9	2737	gi|6755714	Transgelin (TAGLN)	27	333	100	22 575	8.85	0.98	1.97	0.004	Actin cross-linking/gelling protein
10	1431	gi|2078001	Vimentin (VIM)	27	296	100	53 687	5.05	0.84	1.79	0.030	Vimentin is attached to the nucleus, ER and mitochondria
11	2250	gi|148688796	Lectin, galactose binding, soluble 3, (LGALS3)	16	419	100	27 514	8.47	0.82	1.77	0.019	Extracellular matrix organization
12	961	gi|76779273	Heat shock 60 kDa protein 1 (HSPD1)	26	329	100	60 955	5.91	−0.79	1.73	0.008	Chaperone
13	600	gi|7305339	Outer dense fiber protein 2 (ODF2)	22	76	99.68	95 541	7.52	−0.75	1.68	0.029	Maintains sperm morphology and infertility
14	528	gi|18079339	Aconitate hydratase, mitochondrial precursor (ACO2)	30	356	100	85 463	8.08	0.71	1.64	0.002	Catalyzes the isomerization of citrate to isocitrate via *cis*-aconitate
15	2126	gi|148676670	Heat shock protein 5, isoform CRA_b (HSPA5)	23	291	100	72 422	5.07	−0.66	1.58	0.036	Plays a role in facilitating the assembly of multimeric protein complexes inside the ER

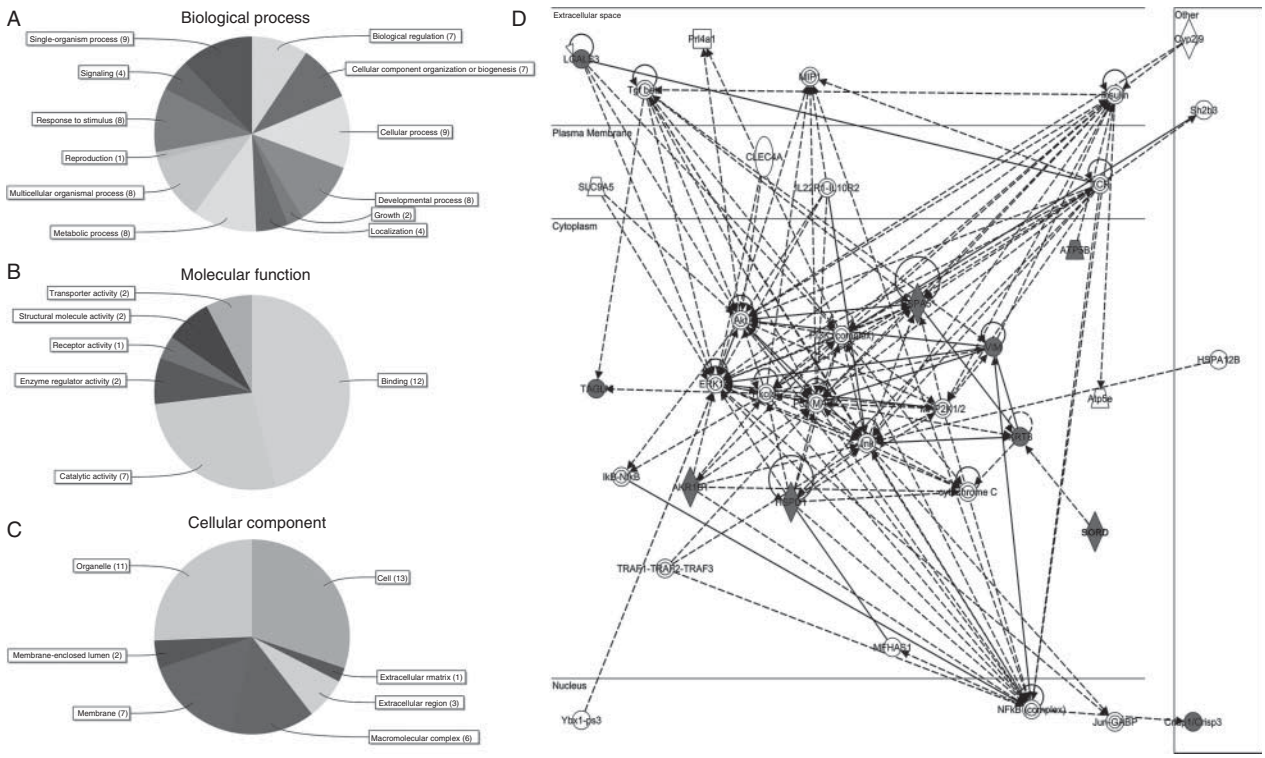

Figure 2 Gene ontology and pathway analysis of the identified DEPs. The pie charts depict the DEPs classified according to (A) major biological process categories, (B) major molecular function categories and (C) cellular component categories. (D) Network enriched for the DEPs between the treated and control samples based on Ingenuity Pathway Analysis. Nodes with a red background are proteins detected in the proteomic analysis. Lines indicate interactions, with the arrowheads indicating directionality. The absence of arrowheads refers to a binding interaction, whereas the dotted lines indicate an inferred or indirect interaction.

Nicotine inhibits tyrosine phosphorylation level in capacitated spermatozoa via downregulated seminal fructose concentration

Among all of the identified DEPs, SORD has long been considered to be an important metabolic enzyme in the sperm maturation process alongside the epididymal lumen (Frenette *et al*. 2006, Katoh *et al*. 2014). SORD participates in carbohydrate metabolism, converting sorbitol into fructose, the important energy source for spermatozoa. Fructose concentration in mouse semen was measured using spectrophotometry, and the results indicated that nicotine treatment significantly attenuated the fructose concentration in seminal plasma as expected (Fig. 3A, $P=0.016$). To further investigate the effects of nicotine on sperm maturation, *in vitro* capacitation of spermatozoa isolated from the cauda epididymis of nicotine-treated and control mice was performed, and tyrosine phosphorylation levels were analyzed by western blotting. As shown in Fig. 3B, tyrosine phosphorylation levels in the nicotine-treated group were significantly lower than those in the control group after *in vitro* capacitation (Fig. 3C, $P=0.001$). To further verify the effects of seminal fructose on *in vitro* sperm capacitation, we replaced glucose in EKRB with a gradient concentration of fructose and performed *in vitro* sperm capacitation. A western blot of tyrosine phosphorylation revealed that deficient fructose in EKRB significantly downregulated tyrosine phosphorylation levels, indicating the impaired sperm capacitation process (Fig. 3D). These results verified the importance of the energy source in the *in vitro* sperm capacitation, and nicotine may inhibit this process via downregulated seminal fructose concentration.

Nicotine attenuates the expression level of SORD in epididymosomes

To investigate the SORD expression pattern during sperm maturation, the distribution of SORD in the mouse epididymis from the control and nicotine-treated groups was observed by IF. The caput, corpus and cauda epididymides were all observed (Fig. 4A), but we found that SORD was mainly expressed in the cauda epididymis. As a consequence, only the microphotographs of the cauda epididymis from the two groups were included in Fig. 4B. Immunohistological localization indicated that SORD was mainly detected in the cauda epididymis region and in the spermatozoa. Besides, the fluorescence signal of SORD in the epididymal lumen was elevated significantly by

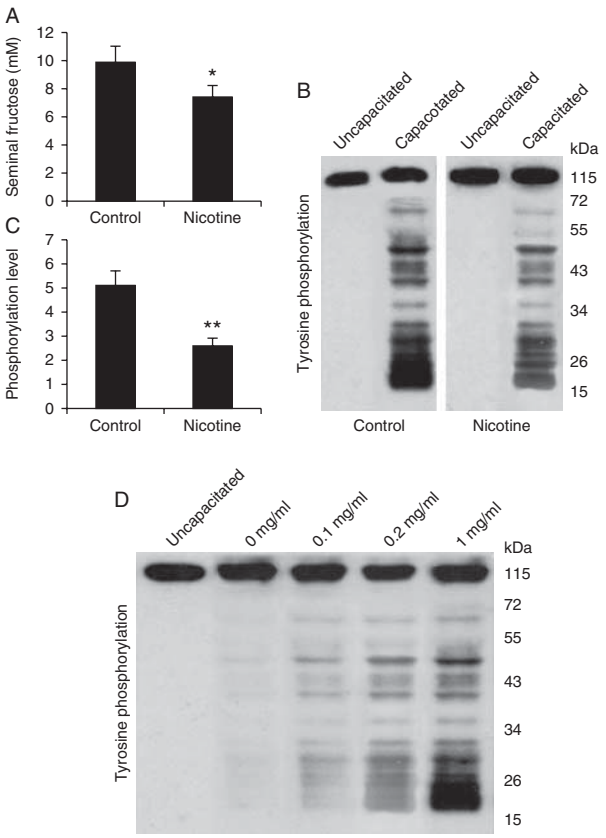

Figure 3 *In vitro* capacitation of spermatozoa from nicotine-treated and control mice. (A) Fructose concentration in semen from nicotine-treated and control mice. (B) Tyrosine phosphorylation in the mouse spermatozoa from nicotine-treated and control mice after *in vitro* capacitation ($n=3$). The band at 115 kD represents a protein that was tyrosine-phosphorylated before and after capacitation, and this band was not considered when calculating the tyrosine phosphorylation level. (C) Histogram representing the tyrosine phosphorylation level in the mouse spermatozoa from nicotine-treated and control mice after *in vitro* capacitation. (D) Tyrosine phosphorylation in the mouse spermatozoa undergone *in vitro* capacitation using EKRB with different concentrations of fructose ($n=3$). * indicates significant differences at $P<0.05$ and ** indicates significant differences at $P<0.01$.

nicotine treatment. Epididymosomes are secreted by the epididymal epithelium and transfer proteins from the epididymal fluid to the sperm surface (Fig. 4C). SORD was found to be present in the epididymosomes and to participate in the polyol pathway in the epididymal fluid (Fig. 4D). As a result, the epididymosomes were also stained by the CD52 antibody that distinguishes epididymosomes and spermatozoa. The IF results indicated that nicotine significantly decreased the distribution of epididymosomes in the cauda epididymis region (Fig. 4B, third row), suggesting that the secretory functions of the epididymis were impaired by nicotine treatment. Meanwhile, nicotine-induced low expression of SORD was mainly located in the epididymosomes and may be a result of attenuated seminal fructose concentration.

Nicotine induces hyper-methylation in the promoter region of Sord

DNA methylation analysis was performed in the promoter region of the *Sord* gene based on the following definitions: CpG islands are defined as DNA sequences of at least 200 bp with a GC content above 50% and an observed/expected ratio of CpG dinucleotides above

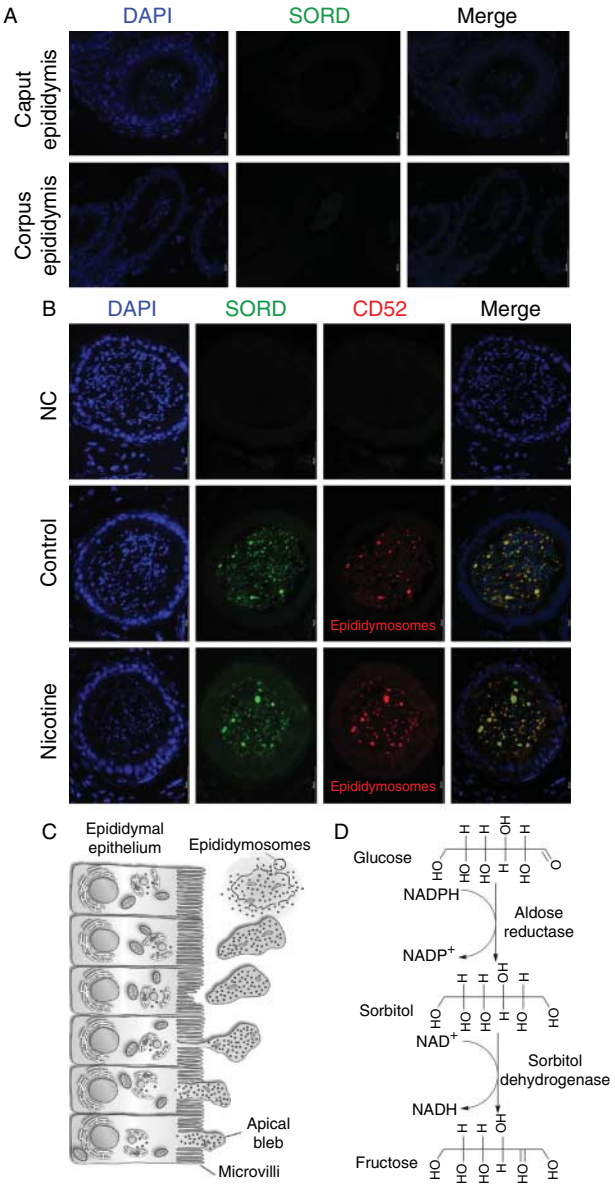

Figure 4 Distribution of SORD in the mouse epididymis from control and nicotine-treated mice. (A) Staining of SORD (green) and DNA (blue) in the mouse caput and corpus epididymides. (B) Staining of SORD (green), CD52 (red) and DNA (blue) in cauda epididymal samples from the two groups. The upper row indicates the negative control, and the next two rows reveal the expression of SORD and CD52 in the control and nicotine-treated testis samples. (C) Schematic representation of apocrine secretion in principal cells of the epididymis and epididymosomes. (D) Schematic representation of the polyol pathway.

0.6. Based on these definitions, the promoter region of mouse *Sord* consisted of four fragments of CpG islands (Fig. 5A). We further investigated the CpG islands by designing primers flanking a 268 bp DNA fragment for bisulfite sequencing analysis. The sequencing information confirmed the presence of 20 CpG islands in the analyzed fragment. Purified DNA samples extracted from epididymal tissue were treated with bisulfite, BSP analysis of methylation patterns was performed in the promoter region of *Sord*. Figure 5B and C illustrates the DNA methylation status of the analyzed fragments in the epididymis from nicotine-treated and control groups. Statistical analysis revealed that the relative methylation levels in the control and nicotine-treated groups were 13.05 ± 2.15 and $24.53 \pm 3.32\%$, respectively. The BSP results indicated that the DNA methylation level of the *Sord* promoter region was elevated significantly ($P=0.001$) in the nicotine-treated group. The Crl-2053 cell line was derived from the testis of the BALB/c mouse and can be used to verify whether the expression of mouse *Sord* can be regulated by DNA methylation level in the specific region. Subsequent verification in the Crl-2053 cell line indicated that 5′-aza-dC treatment attenuated the DNA methylation level in the *Sord* promoter region, and the expressive levels of both *Sord* mRNA and SORD were elevated in the 5′-aza-dC-treated groups with a dose effect (Fig. 5D). These results confirmed that *Sord* can be epigenetically modified with DNA methylation in the promoter region. The expressive level of DNA methyltransferase 3A (DNMT3A) was also observed in the epididymis of nicotine-treated and control mice (Fig. 5E). Western blot analysis revealed that nicotine treatment significantly upregulated DNMT3A levels in the mouse epididymis (Fig. 5F, $P=0.001$), which may be the molecular base for the epigenetic modifications caused by nicotine.

Discussion

The hazardous effects of tobacco smoking on male fertility have long been studied but the underlying molecular mechanism remains vague (Dai *et al.* 2015*b*).

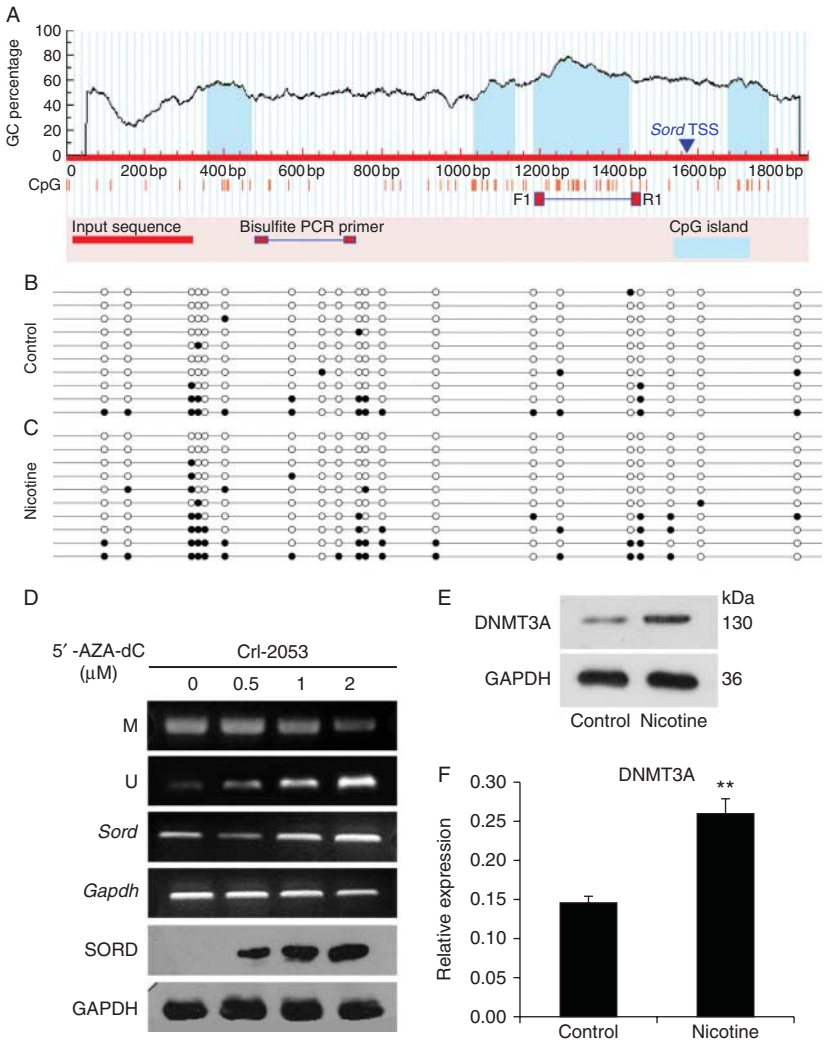

Figure 5 DNA methylation analysis within the promoter region of mouse *Sord*. (A) CpG islands were predicted and BSP primers were designed using the MethPrimer tool. CpG islands are indicated by blue background and BSP primers flanking a 268 bp PCR product are indicated by red stripes. (B) The CpG methylation status of the *Sord* promoter region in the mouse epididymis from control group ($n=5$). Each spot indicates one methylation site (CpG) and the black spots indicate methylated Cs. (C) CpG methylation status of the *Sord* promoter region in the mouse epididymis from the nicotine-treated group ($n=5$). (D) Verification of epigenetic regulation in the Crl-2053 cell line. Panels 1 and 2 show the MSP results for primers designed for methylated and unmethylated sites in Crl-2053 cells treated with 5′-aza-dC in a gradient of concentrations. Panels 3 and 5 show the real-time PCR and western blot analyses of *Sord* expression level in the Crl-2053 cell line. (E) Western blotting films of DNMT3A in the mouse epididymis from the control and nicotine-treated groups ($n=3$). (F) Histogram of the western blot results of DNMT3A in the mouse epididymis from the control and nicotine-treated groups. ** indicated significant differences at $P<0.01$.

Our previous study showed that the mouse epididymis experienced oxidative stress following cigarette smoke exposure (Zhu *et al*. 2013). We assume that heavy metals (e.g. cadmium, lead) but not nicotine are mainly responsible for the oxidative stress caused by tobacco smoke. Considering the complexity of the component in tobacco smoke, our study aimed to elaborate the toxicological effects of nicotine on the protein profile of the mouse epididymis. To achieve this aim, we created a mouse model by i.p. injection of sexually mature male mice with free-base nicotine and found no significant alterations in the weight, length or thicknesses of epididymal lumen between the epididymal samples from the two groups (data not shown). Proteomic analysis revealed 15 identified proteins with expressive levels that differed between the epididymis of the nicotine-treated and control groups. Bioinformatic analyses indicated that most DEPs were related to molecular transportation networks and the polyol pathway. Among the identified DEPs, HSPD1 and GRP78 chaperone proteins were expressed at the surface of oviduct epithelial cells and can be transferred to spermatozoa (Boilard *et al*. 2004, Lachance *et al*. 2007), and downregulation of these two chaperones may prompt a hindered sperm maturation process induced by nicotine. The molecular transportation functions of the epididymis are mainly correlated with the minute vesicular bodies present in the epididymal luminal fluid called epididymosomes that transfer essential proteins to the sperm plasma membrane during the sperm maturation process (Saez *et al*. 2003, Sullivan *et al*. 2005). In our study, nicotine was found to reduce the quantity of epididymosomes in the mouse epididymal lumen, which can be considered a direct embodiment of impaired epididymal secretive functions.

Through the female genital tract, spermatozoa undergo a series of structural and functional changes referred to as sperm capacitation (Aitken 2011). The biochemical modifications of spermatozoa during capacitation include modulation of enzyme activities, membrane modifications and protein tyrosine phosphorylation (De Jonge 2005). These tyrosine phosphorylation modifications are only partially known at the molecular level, but require an adequate supply of sufficient energy sources (Mukai & Okuno 2004, Ferramosca & Zara 2014), mainly including fructose (Cao *et al*. 2009) and glucose (Urner & Sakkas 2003), the metabolic products (ATP and NADPH) of which appear to participate in signaling pathways by supporting the precise onset of protein tyrosine phosphorylation in the sperm flagellum leading to successful fertilization. The polyol pathway is related to epididymosomes that modulate sperm motility during the epididymal transit, which involves aldose reductase (ALDR) that uses NADPH to reduce glucose to sorbitol. Afterwards, SORD used NAD^+ to generate fructose (Fig. 5A; Visconti 2012). Our study reveals that *Sord*, a key gene in the polyol pathway, is a novel DNA methylation-regulated gene and nicotine treatment induces the downregulation of *Sord* expression via hyper-methylation in its promoter region. The tyrosine phosphorylation level after *in vitro* sperm capacitation was measured to observe the effects of lower seminal fructose because of the dependence of energy sources in the modification. Insufficient supply of energy sources induced by the downregulation of SORD significantly inhibits tyrosine phosphorylation level in spermatozoa undergone *in vitro* capacitation, and this effect may be a marker of the impaired sperm capacitation process. Further test for the ability of mouse sperm to undergo fertilization can provide more valid evidence for the impairment of sperm capacitation by nicotine.

In summary, we have discovered alterations in the protein expression profile that involved in the molecular transportation process and the polyol pathway in the mouse epididymis due to *in vivo* nicotine exposure. Reduced expression of SORD in the cauda epididymis, specifically in epididymosomes, has also been observed due to DNA hyper-methylation in the *Sord* promoter region. Nicotine-induced reduced expression of *Sord* involves in impaired secretory functions of the epididymis and thus inhibits tyrosine phosphorylation level in capacitated spermatozoa. These effects may outline the etiology of the impaired capacitation of spermatozoa and provide a foundation for further analyses of the effects of nicotine on sperm maturation and capacitation.

Declaration of interest

The authors declare that there is no conflict of interest that could be perceived as prejudicing the impartiality of the research reported.

Funding

This work was supported by a grant from the Shanghai Natural Science Foundation (grant no. 15ZR1423000) and the Shanghai Jiao Tong University Medical Engineering Joint Project (YG2012MS56).

References

Aitken RJ 2011 The capacitation-apoptosis highway: oxysterols and mammalian sperm function. *Biology of Reproduction* **85** 9–12. (doi:10.1095/biolreprod.111.092528)

Boilard M, Reyes-Moreno C, Lachance C, Massicotte L, Bailey J, Sirard M-A & Leclerc P 2004 Localization of the chaperone proteins GRP78 and HSP60 on the luminal surface of bovine oviduct epithelial cells and their association with spermatozoa. *Biology of Reproduction* **71** 1879–1879. (doi:10.1095/biolreprod.103.026849)

Bornman M, Kok E, du Plessis D & Otto B 1989 Clinical features of patients with detached ciliary tufts in semen. *Andrologia* **21** 18. (doi:10.1111/j.1439-0272.1988.tb00728.x)

Cao W, Aghajanian HK, Haig-Ladewig LA & Gerton GL 2009 Sorbitol can fuel mouse sperm motility and protein tyrosine phosphorylation via sorbitol dehydrogenase. *Biology of Reproduction* **80** 124–133. (doi:10.1095/biolreprod.108.068882)

Cooper TG & Yeung C-H 2006 Sperm maturation in the human epididymis. In *The Sperm Cell. Production, Maturation, Fertilization, Regeneration*, pp 72–107. Cambridge, UK: Cambridge University Press.

Dacheux J-L & Dacheux F 2014 New insights into epididymal function in relation to sperm maturation. *Reproduction* **147** R27–R42. (doi:10.1530/REP-13-0420)

Dai J-B, Wang Z-X & Qiao Z-D 2015*a* The hazardous effects of tobacco smoking on male fertility. *Asian Journal of Andrology* **17** 954–960. (doi:10.4103/1008-682X.150847)

Dai J, Zhan C, Xu W, Wang Z, Nie D, Zhao X, Zhang D, Gu Y, Wang L, Chen Z & Qiao Z 2015*b* Nicotine elevates sperm motility and induces Pfn1 promoter hypomethylation in mouse testis. *Andrology* **3** 967–978. (doi:10.1111/andr.12072)

De Jonge C 2005 Biological basis for human capacitation. *Human Reproduction Update* **11** 205–214. (doi:10.1093/humupd/dmi010)

Editorial 2014 Clearing the smoke. *Nature Neuroscience* **17** 10–13. (doi:10.1038/nn.3777)

Ezzatabadipour M, Azizollahi S, Sarvazad A, Mirkahnooj Z, Mahdinia Z & Nematollahi-Mahani SN 2012 Effects of concurrent chronic administration of alcohol and nicotine on rat sperm parameters. *Andrologia* **44** 330–336. (doi:10.1111/j.1439-0272.2012.01284.x)

Ferramosca A & Zara V 2014 Bioenergetics of mammalian sperm capacitation. *BioMed Research International* **2014** 902–953. (doi:10.1155/2014/902953)

Frenette G, Thabet M & Sullivan R 2006 Polyol pathway in human epididymis and semen. *Journal of Andrology* **27** 233–239. (doi:10.2164/jandrol.05108)

Gaur D, Talekar M & Pathak V 2007 Effect of cigarette smoking on semen quality of infertile men. *Singapore Medical Journal* **48** 119–123.

Girela JL, Gil D, Johnsson M, Gomez-Torres MJ & De Juan J 2013 Semen parameters can be predicted from environmental factors and lifestyle using artificial intelligence methods. *Biology of Reproduction* **88** 99–99. (doi:10.1095/biolreprod.112.104653)

González-Jiménez M & Villanueva-Díaz C 2006 Epididymal stereocilia in semen of infertile men: evidence of chronic epididymitis? *Andrologia* **38** 26–30.

Jana K, Samanta PK & De DK 2010 Nicotine diminishes testicular gametogenesis, steroidogenesis, and steroidogenic acute regulatory protein expression in adult albino rats: possible influence on pituitary gonadotropins and alteration of testicular antioxidant status. *Toxicological Science* **116** 647–659. (doi:10.1093/toxsci/kfq149)

Jones R 1999 To store or mature spermatozoa? The primary role of the epididymis *International Journal of Andrology* **22** 57–66. (doi:10.1046/j.1365-2605.1999.00151.x)

Künzle R, Mueller MD, Hänggi W, Birkhäuser MH, Drescher H & Bersinger NA 2003 Semen quality of male smokers and nonsmokers in infertile couples. *Fertility and Sterility* **79** 287–291. (doi:10.1016/S0015-0282(02)04664-2)

Katoh Y, Takebayashi K, Kikuchi A, Iki A, Kikuchi K, Tamba M, Kawashima A, Matsuda M & Okamura N 2014 Porcine sperm capacitation involves tyrosine phosphorylation and activation of aldose reductase. *Reproduction* **148** 389–401. (doi:10.1530/REP-14-0199)

Lachance C, Bailey JL & Leclerc P 2007 Expression of Hsp60 and Grp78 in the human endometrium and oviduct, and their effect on sperm functions. *Human Reproduction* **22** 2606–2614. (doi:10.1093/humrep/dem242)

Matta SG, Balfour DJ, Benowitz NL, Boyd RT, Buccafusco JJ, Caggiula AR, Craig CR, Collins AC, Damaj MI, Donny EC *et al.* 2007 Guidelines on nicotine dose selection for *in vivo* research. *Psychopharmacology* **190** 269–319. (doi:10.1007/s00213-006-0441-0)

Mukai C & Okuno M 2004 Glycolysis plays a major role for adenosine triphosphate supplementation in mouse sperm flagellar movement. *Biology of Reproduction* **71** 540–547. (doi:10.1095/biolreprod.103.026054)

Oyeyipo IP, Raji Y, Emikpe BO & Bolarinwa AF 2011 Effects of nicotine on sperm characteristics and fertility profile in adult male rats: a possible role of cessation. *Journal of Reproduction & Infertility* **12** 201–207.

Pacifici R, Altieri I, Gandini L, Lenzi A, Passa AR, Pichini S, Rosa M, Zuccaro P & Dondero F 1995 Environmental tobacco-smoke-nicotine and cotinine concentration in Semen. *Environmental Research* **68** 69–72. (doi:10.1006/enrs.1995.1009)

Pfaffl M, Tichopad A, Prgomet C & Neuvians T 2004 Determination of stable housekeeping genes, differentially regulated target genes and sample integrity: BestKeeper – Excel-based tool using pair-wise correlations. *Biotechnology Letters* **26** 509–515. (doi:10.1023/B:BILE.0000019559.84305.47)

Ramlau-Hansen C, Thulstrup AM, Aggerholm AS, Jensen MS, Toft G & Bonde JP 2007 Is smoking a risk factor for decreased semen quality? A cross-sectional analysis *Human Reproduction* **22** 188–196. (doi:10.1093/humrep/del364)

Rodriguez C, Kirby J & Hinton B 2002 The Epididymis: From Molecules to Clinical Practice, Springer, Berlin.

Saez F, Frenette G & Sullivan R 2003 Epididymosomes and prostasomes: their roles in posttesticular maturation of the sperm cells. *Journal of Andrology* **24** 149–154. (doi:10.1002/j.1939-4640.2003.tb02653.x)

Sullivan R, Saez F, Girouard J & Frenette G 2005 Role of exosomes in sperm maturation during the transit along the male reproductive tract. *Blood Cells, Molecules & Diseases* **35** 1–10. (doi:10.1016/j.bcmd.2005.03.005)

Trummer H, Habermann H, Haas J & Pummer K 2002 The impact of cigarette smoking on human semen parameters and hormones. *Human Reproduction* **17** 1554–1559. (doi:10.1093/humrep/17.6.1554)

Urner F & Sakkas D 2003 Protein phosphorylation in mammalian spermatozoa. *Reproduction* **125** 17–26. (doi:10.1530/rep.0.1250017)

Visconti P 2012 Sperm bioenergetics in a nutshell. *Biology of Reproduction* **87** 72–26. (doi:10.1095/biolreprod.112.104109)

Yach D 2014 The origins, development, effects, and future of the WHO Framework Convention on Tobacco Control: a personal perspective. *Lancet* **383** 1771–1779. (doi:10.1016/S0140-6736(13)62155-8)

Zhu Z, Xu W, Dai J, Chen X, Zhao X, Fang P, Yang F, Tang M, Wang Z & Wang L 2013 The alteration of protein profile induced by cigarette smoking via oxidative stress in mice epididymis. *International Journal of Biochemistry & Cell Biology* **45** 571–582. (doi:10.1016/j.biocel.2012.12.007)

Received 18 August 2015
First decision 16 September 2015
Revised manuscript received 3 December 2015
Accepted 8 December 2015